

# A hit expansion of 3-benzamidopyrazine-2-carboxamide: Toward inhibitors of prolyl-tRNA synthetase with antimycobacterial activity

Vinod Sukanth Kumar Pallabothula<sup>1</sup>  | Nechirwan Taimur Abdalrahman<sup>1</sup> | Matteo Mori<sup>2</sup>  | Amir Hossein Fekri<sup>1</sup> | Ondřej Jandourek<sup>1</sup>  | Klára Konečná<sup>1</sup>  | Pavla Paterová<sup>3</sup>  | Martin Novák<sup>4</sup>  | Paulína Dudášová-Hatoková<sup>1</sup>  | Petra Štěrbová-Kovaříková<sup>1</sup>  | Carlo Castellano<sup>5</sup>  | Fiorella Meneghetti<sup>2</sup>  | Stefania Villa<sup>2</sup>  | Jiří Kuneš<sup>1</sup>  | Martin Juhás<sup>1,6</sup>  | Jan Zitko<sup>1</sup> 

<sup>1</sup>Department of Clinical Microbiology, University Hospital Hradec Králové, Hradec Králové, Czech Republic

<sup>2</sup>Faculty of Pharmacy in Hradec Králové, Charles University, Hradec Králové, Czech Republic

<sup>3</sup>Department of Pharmaceutical Sciences, University of Milan, Milan, Italy

<sup>4</sup>Biomedical Research Centre, University Hospital Hradec Králové, Hradec Králové, Czech Republic

<sup>5</sup>Department of Chemistry, University of Milan, Milan, Italy

<sup>6</sup>Faculty of Science, University of Hradec Králové, Hradec Králové, Czech Republic

## Correspondence

Vinod Sukanth Kumar Pallabothula and Jan Zitko, Faculty of Pharmacy in Hradec Králové, Charles University, Ak. Heyrovského 1203, Hradec Králové 500 03, Czech Republic.  
Email: [pallabov@faf.cuni.cz](mailto:pallabov@faf.cuni.cz) and [jan.zitko@faf.cuni.cz](mailto:jan.zitko@faf.cuni.cz)

## Funding information

Supported by Ministry of Health of the Czech Republic, Grant/Award Number: NU21-05-00482 (grant to J. Z.); The publication was supported by the research project 2200/04/2024-2026 as part of the "Competition for 2024-2026 Postdoctoral Job Positions at the University of Hradec Králové", at the Faculty of Science, University of Hradec Králové (grant to M. J.); Grant Agency of Charles University with Project GA UK No. 349 721 and Charles University with project SVV 260 666

## Abstract

This study presents an exploration of the chemical space around derivatives of 3-benzamidopyrazine-2-carboxamides, previously identified as potent antimycobacterial compounds with predicted binding to mycobacterial prolyl-transfer RNA synthetase. New urea derivatives (Series-1) were generally inactive, probably due to their preference for *cis-trans* conformation (confirmed by density functional theory calculations and experimentally by nuclear overhauser effect spectroscopy NMR). Series-2 (3-benzamidopyrazine-2-carboxamides with disubstituted benzene ring) demonstrated that substituents larger than fluorine are not tolerated in the *ortho* position of the benzene ring. This series brought two new compounds (**21**: R = 2-F, 4-Cl and **22**: R = 2-F, 4-Br) with *in vitro* activity against *Mycobacterium tuberculosis* H37Rv as well as multidrug-resistant clinical isolates, with minimum inhibitory concentration ranging from 6.25 to 25 µg/mL. The lactone-type derivatives 4*H*-pyrazino[2,3-*d*][1,3]oxazin-4-ones (Series-3) were inactive, but solvent stability studies of compound **29** indicated that they might be developed to usable lactone prodrugs of inhibitors of mycobacterial aspartate decarboxylase (PanD).

## KEYWORDS

3-aminopyrazinamide, antimycobacterial, hit expansion, multidrug-resistant, prolyl-tRNA synthetase

This is an open access article under the terms of the [Creative Commons Attribution](https://creativecommons.org/licenses/by/4.0/) License, which permits use, distribution and reproduction in any medium, provided the original work is properly cited.

© 2024 The Authors. *Archiv der Pharmazie* published by Wiley-VCH GmbH on behalf of Deutsche Pharmazeutische Gesellschaft.

## 1 | INTRODUCTION

Prolyl-transfer RNA (tRNA) synthetase (ProRS), one of the enzymes of the aminoacyl-tRNA synthetases family, is responsible for the ATP-dependent attachment of L-Proline (Pro) to its tRNA molecule. Natural alkaloid febrifugine (Figure 1a) and its derivatives, including halofuginone (HFG, Figure 1b), are ProRS inhibitors that occupy both L-Pro and tRNA binding sites of the enzyme.<sup>[1]</sup> They exhibit excellent properties against malaria, fibroproliferative diseases, or cancer.<sup>[2–5]</sup> However, both the antimalarial and antifibrotic activity of HFG are negatively affected by the accumulation of Pro due to the proline-competitive nature of the binding. Considering this evidence, proline-noncompetitive or proline-dependent inhibitors could overcome this “resistance” mechanism.<sup>[3]</sup> Bersiporocin (DWN12088, Figure 1c), as an inhibitor of human ProRS (hsProRS), is in Phase 2 clinical trial (ClinicalTrials.gov ID NCT05389215) for the treatment of idiopathic pulmonary fibrosis.<sup>[6]</sup>

Other inhibitors of hsProRS were reported by Adachi et al. (Figure 1d)<sup>[7,8]</sup> and are based on the structure of substituted 3-aminopyrazine-2-carboxamide. In contrast to the previously mentioned structures Figure 1a–c, the 3-amino-pyrazinamide-based inhibitors miss the proline-like fragment and, therefore, are not proline-competitive. In our previous papers, we showed that simplified derivatives of the Adachi ligand missing the bulky substituent on the

C2 carboxamide and carbonyl oxygen in position 3 (Figure 1e) are still effective ATP-competitive and Pro-dependent binders of hsProRS (as confirmed by thermal shift assays and crystallographic structures).<sup>[9]</sup> In another paper, the reintroduction of the carbonyl oxygen and change of the substitution pattern on the benzene ring resulted in compounds with low human hepatoblastoma cell-line cytotoxicity (a possible indicator of decreased affinity to hsProRS), and substantial micromolar antimycobacterial activity (as a possible indicator of increased affinity to mycobacterial ProRS [mtProRS]).<sup>[10]</sup> These compounds, *para*-substituted with short alkyl or halogen, showed excellent and consistent antimycobacterial activity against *Mycobacterium tuberculosis* H37Ra and multidrug-resistant (MDR) clinical isolates. Molecular docking followed by molecular dynamics confirmed mtProRS as a probable target.<sup>[10]</sup> These compounds were designated as the first generation of probable mtProRS inhibitors with whole-cell antimycobacterial activity (Figure 1f).

The aim of the current study is the structural hit-expansion of the antimycobacterial compounds of the first generation for a better understanding of the structure–activity relationships (SAR). We proposed, synthesized, and tested three series of compounds (Figure 2) based on the following rationale: Series-1 contains derivatives with a urea linker, derived by extending the linker by one atom and preserving the carbonyl oxygen at the same time. Urea derivatives are commonly used in medicinal chemistry<sup>[11]</sup>; some

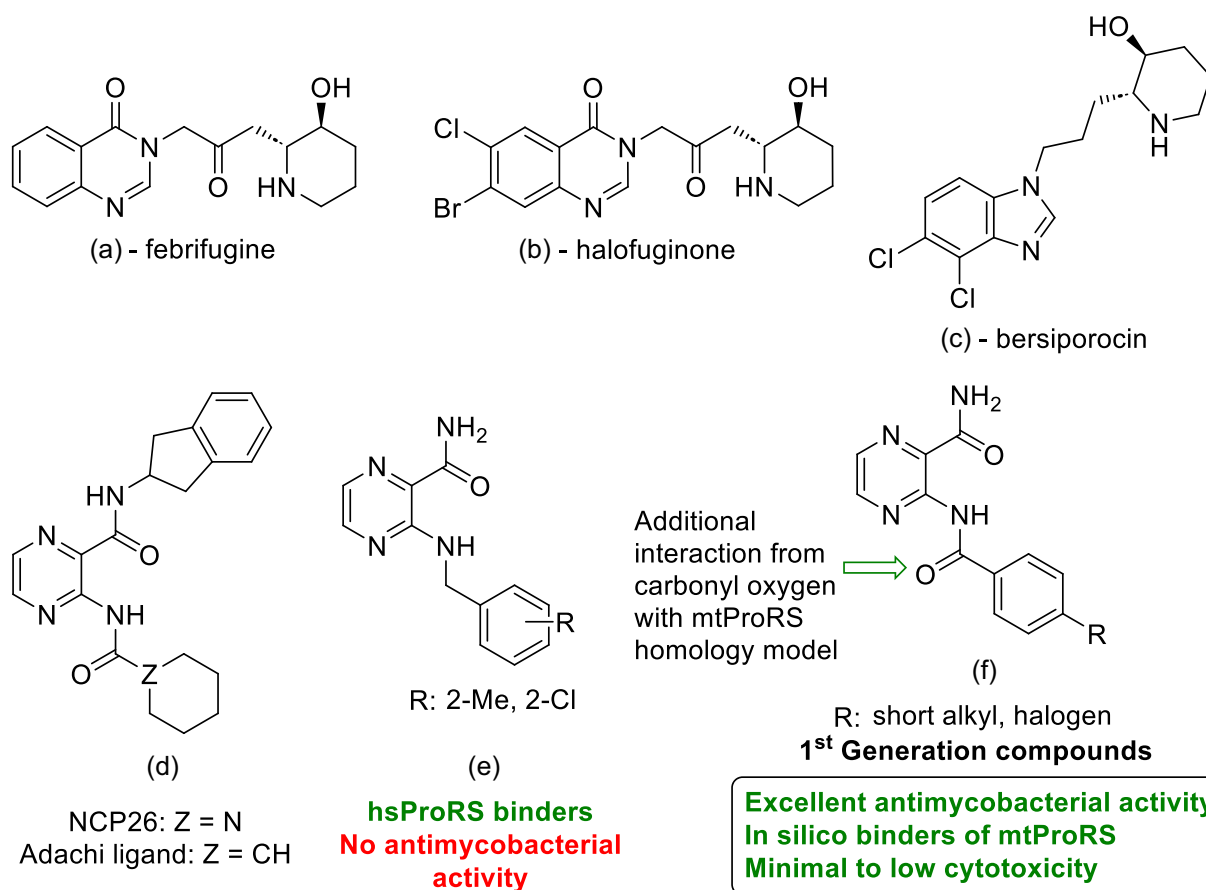


**FIGURE 1** Inhibitors or binders of prolyl-tRNA synthetase (ProRS). (a) Febrifugine; (b) halofuginone; (c) bersiporocin; (d) NCP26 and Adachi ligand; (e) hsProRS binders with no antimycobacterial activity; (f) 1<sup>st</sup> generation compounds.

pyrazinyl ureas were previously reported for antimycobacterial activity.<sup>[12]</sup> Series-2 combines the *para* substitution from the first generation (positively linked with antimycobacterial activity) with *ortho* substitution positively linked with hsProRS binding (Figure 1e). Series-3 are O-isosteres (lactones) of the heteroaromatic lactams published alongside the first generation of compounds.<sup>[10]</sup>

## 2 | RESULTS AND DISCUSSION

### 2.1 | Chemistry

#### 2.1.1 | Synthesis of urea derivatives (1–17)

Synthesis of urea derivatives 1–17 involved three steps, as shown in Scheme 1, starting with partial hydrolysis (a) of pyrazinecarbonitrile (I) to pyrazinecarboxamide (II) using hydrogen peroxide in water under basic conditions with pH control. The pH had to be maintained around 9.0 and the temperature to be under 55°C to prevent complete hydrolysis.<sup>[13]</sup> The crude product was filtered as yellow crystals and recrystallized from hot ethanol to obtain white crystals with a 60% yield. The 3-chloropyrazine-2-carboxamide (II) underwent nucleophilic substitution of chlorine with ammonia in anhydrous

methanol (b). The reaction was first attempted at the boiling point of methanol, but the conversion rate was low, and the ammonia volatility was an issue. Therefore, to increase the speed and rate of conversion, the reaction was performed at 120°C in a pressurized tube using a microwave (MW) reactor. After cooling, the product 3-aminopyrazine-2-carboxamide (III) precipitated in sufficient purity and was used in the next step without further purification. N.B. The substitution (b) was first attempted with an aqueous solution of ammonia (25% m/m), but the yields were very low, partially due to the low solubility of II in water.

To obtain the final urea derivatives, 3-aminopyrazine-2-carboxamide (III) reacted with various “R” substituted phenyl isocyanates (c) under MW heating using anhydrous acetonitrile (MeCN) as a solvent. Other solvents like hexane (Hex) used by Bouz et al.<sup>[12]</sup> or tetrahydrofuran (THF) were not used due to minimal or low reactivity during our optimization steps. The reaction was also attempted in neat conditions (without solvent), but carbonizations occurred, requiring higher amounts of the substituted phenyl isocyanate. Many of the obtained disubstituted ureas were highly insoluble in the reaction mixture and in many common organic solvents. Hence, they were purified simply by filtration and sequential washing with water (removing the excess isocyanate) and with organic solvents such as hexane, dichloromethane, or acetone. The ureas containing alkyl/

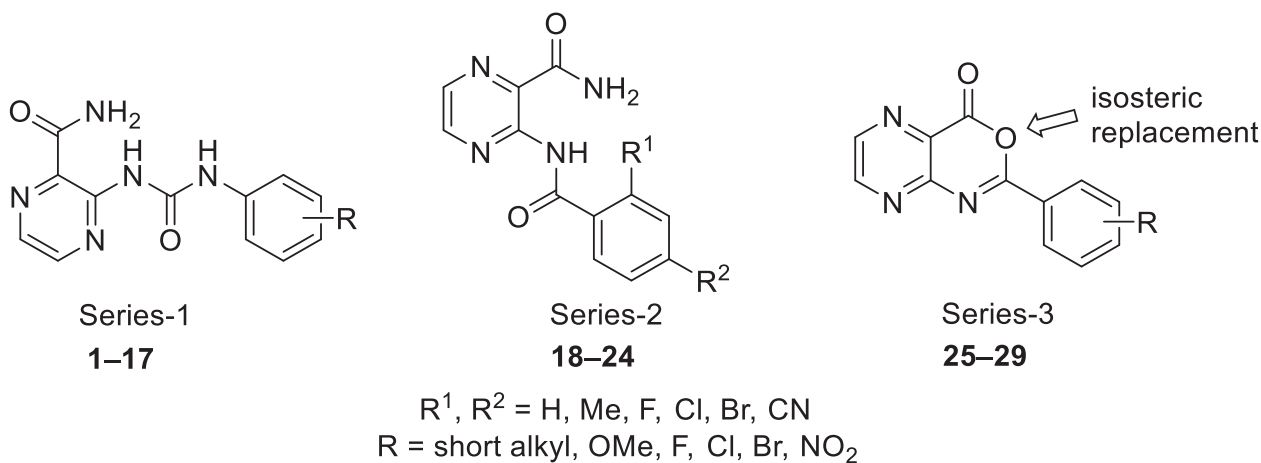
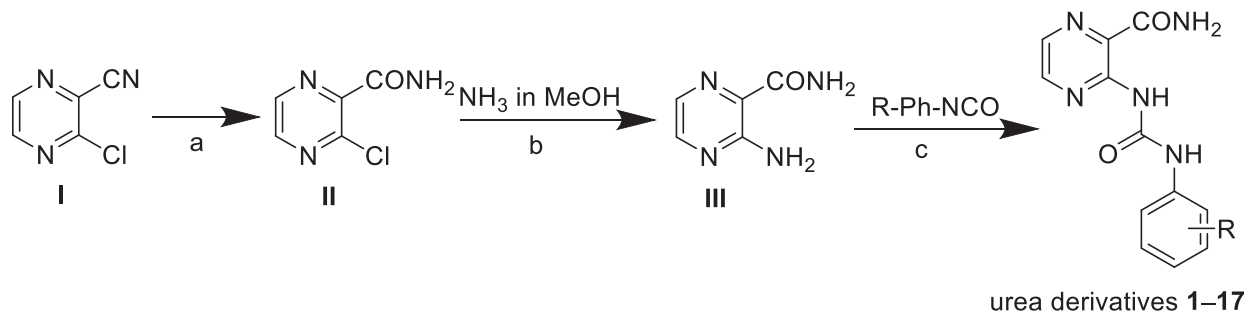


**FIGURE 2** Currently developed series. The arrow in Series-3 indicates the position of isosteric replacement in comparison with previously published pteridine derivatives.<sup>[10]</sup>



**SCHEME 1** Synthesis of urea derivatives. Conditions: (a)  $\text{H}_2\text{O}_2$ , pH 9.0 via 8% m/m NaOH,  $\text{H}_2\text{O}$  as a solvent, 55°C for 3.0 h; (b) MW, 7.0 N  $\text{NH}_3$  in MeOH, 120°C for 0.5 h; (c) MW, anhyd. MeCN as solvent, 120°C for 0.5 h.

methoxy substitutions were better soluble and, therefore, purified by automated flash chromatography on silica using a gradient of 0%–100% ethyl acetate (EtOAc) in Hex. All final ureas were subjected to boiling in acetone to remove traces of impurities. If the urea product was partially dissolved in hot acetone, it was recovered from the filtrate by precipitation induced by a small amount of cold hexane. The urea derivatives were isolated as solids with yields ranging from 20% to 30%.

### 2.1.2 | Synthesis of amidic derivatives (18–24)

The synthesis of 3-benzamidopyrazine-2-carboxamides (18–24) was performed as a single-step *N*-acylation of 3-aminopyrazine-2-carboxamide (III) as seen in Scheme 2 with commercially available benzoyl chlorides (2.1 eq.) in anhyd. MeCN at 50°C for 24 h, using pyridine as base. The lower temperature (compared to 70°C used for the *N*-acylation of methyl 3-aminopyrazine-2-carboxylate as described in our previous publication<sup>[10]</sup>) favored the production of monoacylated final products with isolated yields ranging from 70% to 80%. Once the reaction was completed, the crude product was extracted to EtOAc and washed with water to remove pyridine followed by purification in automated flash chromatography using Hex:EtOAc gradient mobile phase.

### 2.1.3 | Synthesis of cyclic derivatives (25–29)

The key intermediates, methyl 3-carboxamidopyrazine-2-carboxylates (V), were prepared as previously reported.<sup>[10]</sup> Briefly, this approach included the intentional overacylation of the 3-amino moiety to produce *N,N*-dibenzoyl derivatives, which were subsequently reduced by hydrazine in isopropanol and THF to monoacylated products. The overacylation required increased reaction temperature (70°C in MeCN) due to the decreased reactivity (nucleophilicity) of the 3-amino group in the 3-aminopyrazine-2-carboxylate compared to 3-aminopyrazine-2-carboxamide (compare with Scheme 2). We speculate that the higher steric hindrance of the methyl ester group caused the decreased reactivity. The crude product was extracted into EtOAc and washed several times with acidified water (a few drops of sulfuric acid in water) to remove the anticipated hydrazide side product.

The key intermediates (V) were cyclized (Scheme 3e) by applying a previously described procedure.<sup>[14]</sup> The ring closure is described in

the literature to happen through the action of dibromotriphenylphosphorane, which is generated in situ by the reaction of 1,2-dibromotetrachloroethane on triphenylphosphine.<sup>[14]</sup> The isolated yields of the cyclization reaction were relatively low, ranging from 10% to 30%, due to low reactivity followed by heavy losses during the purification steps.

## 2.2 | Spectral characterization of final compounds

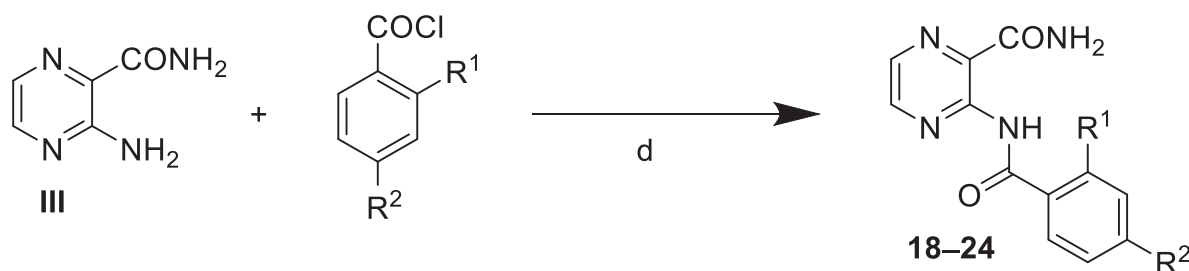
All final compounds were characterized by <sup>1</sup>H and <sup>13</sup>C NMR spectra measured in hexadeuterodimethyl sulfoxide (DMSO-*d*<sub>6</sub>) at ambient temperature (or increased temperature for 1–17 due to low solubility) and compound 25 measured in deuteriochloroform (CDCl<sub>3</sub>), IR spectroscopy, elemental analysis (except fluorine-containing compounds), and melting point. The purity of final compounds containing fluorine atoms was checked by high-performance liquid chromatography (HPLC) analysis followed by characterization using high-resolution mass spectrometry (HRMS); the chromatograms and the HRMS spectra are presented in Supporting Information S2. The analytical data of all final compounds and the intermediates corresponded to the proposed structures.

Description of typical <sup>1</sup>H NMR spectra of final compounds: carboxamide protons (CONH<sub>2</sub>) were observed as two short broad singlets at the 8.7–7.8 ppm range. Ureido protons (NHCONH) were observed as two sharp singlets at 13.0–11.5 ppm, and pyrazine protons were observed as two doublets (*J* = 2.4 Hz) at 8.8–8.2 ppm. NMR spectra of the synthesized compounds are presented in Supporting Information S2.

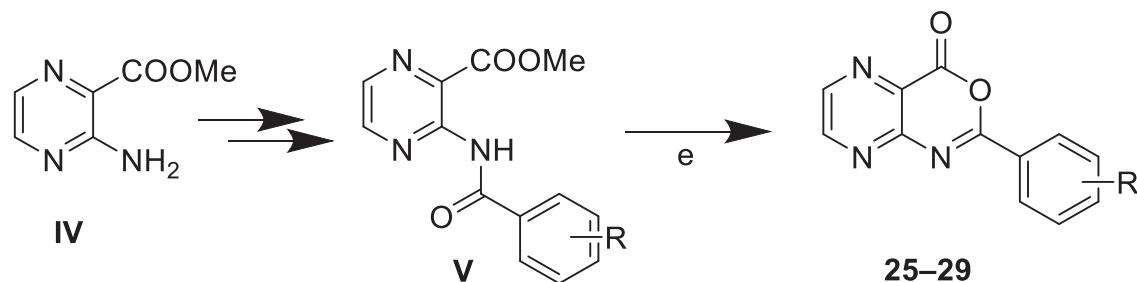
Description of typical IR spectra of final compounds: Strong carbonyl stretching of carboxamide signals was observed from 1665 to 1716 cm<sup>-1</sup>, a sharp signal of NH stretching in the ranges from 3430 to 3480 cm<sup>-1</sup>, broad C–H stretching of aromatic groups from 3200 to 3100 cm<sup>-1</sup>, while the CH signals in the alkyl group from 2950 to 2800 cm<sup>-1</sup>, phenyl C=C stretching in the range from 1620 to 1400 cm<sup>-1</sup>.

## 2.3 | Antimycobacterial activity

All final compounds were screened for whole-cell antimycobacterial activity against *Mtb* H37Ra (avirulent strain), *Mycobacterium smegmatis*, *Mycobacterium aurum*, *Mycobacterium kansasii*, and *Mycobacterium avium*. The results of the antimycobacterial screenings for



**SCHEME 2** Synthesis of amidic derivatives. (d) Anhyd. pyridine as base, anhyd. MeCN as solvent, and 50°C for 24 h.




**SCHEME 3** Synthesis of cyclic derivatives. (e) Triphenylphosphine, 1,2-dibromotetrachloroethane, triethylamine as base, toluene as solvent, and 80°C for 4–6 h.

**TABLE 1** Results of the antimycobacterial screening of Series-1, the urea derivatives.

1–17

Code	R	MIC (µg/mL)					Clog P
		<i>Mycobacterium smegmatis</i>	<i>Mycobacterium aurum</i>	<i>Mycobacterium avium</i>	<i>Mycobacterium kansasii</i>	<i>Mtb H37Ra</i>	
1	H	≥500	≥500	500	≥500	≥500	1.80
2	2-Me	≥500	≥500	≥500	≥500	≥500	1.73
3	3-Me	≥125	≥125	≥125	≥125	≥125	2.29
4	4-Me	≥125	≥125	≥125	≥125	≥125	2.29
5	4-tertBu	≥500	≥500	≥500	62.5	≥500	3.62
6	3-OMe	≥250	≥250	≥250	≥250	≥250	1.72
7	4-OMe	≥500	≥500	≥500	≥500	≥500	1.72
8	2-F	≥500	≥500	250	≥500	≥500	1.50
9	3-F	≥500	≥500	≥500	≥500	≥500	1.95
10	4-F	≥500	≥500	≥500	≥500	≥500	1.95
11	2-Cl	NT	NT	NT	NT	NT	1.96
12	3-Cl	≥125	≥125	≥125	≥125	≥125	2.52
13	4-Cl	≥500	≥500	250	≥500	≥500	2.52
14	2-Br	NT	NT	NT	NT	NT	2.11
15	3-Br	≥125	≥125	≥125	62.5	≥125	2.67
16	4-Br	≥500	≥500	250	≥500	≥500	2.67
17	4-NO <sub>2</sub>	≥500	≥500	62.5	500	≥500	1.59
CIP		0.125	0.015625	1.56	0.125	0.25	-
INH		31.25	3.91	≥500	6.25	0.25	-
RIF		25	0.39	0.125	0.025	0.003125	-

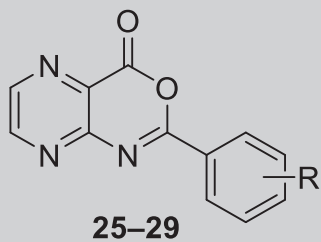
Abbreviations: CIP, ciprofloxacin; Clog P, calc. from ChemDraw v.22.2.0; INH, isoniazid; MIC, minimum inhibitory concentration; NT, not tested due to low solubility in DMSO (stock solutions); RIF, rifampicin.

**TABLE 2** Results of the antimycobacterial screening of Series-2, the amidic derivatives.


**18–24**

Code	R <sup>1</sup>	R <sup>2</sup>	MIC (µg/mL)					Clog P
			<i>Mycobacterium smegmatis</i>	<i>Mycobacterium aurum</i>	<i>Mycobacterium avium</i>	<i>Mycobacterium kansasii</i>	<i>Mtb H37Ra</i>	
18	H	CN	≥125	≥125	≥125	≥125	≥125	0.42
19	Me	F	≥500	≥500	500	500	≥500	1.27
20	F	F	≥125	≥125	≥125	31.25	≥125	0.84
21	F	Cl	62.5	125	62.5	3.91	31.25	1.41
22	F	Br	31.25	62.5	31.25	3.91	31.25	1.56
23	Cl	F	≥125	≥125	≥125	≥125	≥125	0.99
24	Cl	Cl	≥250	≥250	≥250	31.25	≥250	1.56

Abbreviations: Clog P, calc. from ChemDraw v.22.2.0; MIC, minimum inhibitory concentration.

**TABLE 3** Antimycobacterial screening of Series-3, the pyrazinooxazinone derivatives.


**25–29**

Code	R	MIC (µg/mL)					Clog P
		<i>Mycobacterium smegmatis</i>	<i>Mycobacterium aurum</i>	<i>Mycobacterium avium</i>	<i>Mycobacterium kansasii</i>	<i>Mtb H37Ra</i>	
25	4-Me	≥125	≥125	≥125	125	≥125	0.68
26	4-tertBu	250	250	≥500	≥500	≥500	2.00
27	4-OMe	≥500	≥500	≥500	≥500	≥500	0.19
28	2-F	≥500	≥500	≥500	≥500	≥500	0.32
29	4-Cl	≥125	≥125	≥125	62.5	≥125	0.89

Abbreviations: Clog P, calc. from ChemDraw v.22.2.0; MIC, minimum inhibitory concentration.

Series-1, Series-2, and Series-3 are presented in Tables 1, 2, and 3, respectively. The same standards (ciprofloxacin [CIP], isoniazid [INH], rifampicin [RIF]) were used in all antimycobacterial activity determinations, and their minimum inhibitory concentrations (MICs) are presented in Table 1. Selected final compounds were additionally screened against the virulent strain *Mtb H37Rv* and MDR clinical isolates (*Mtb SORO*, *Mtb MATI*, and *Mtb IZAK*); the results are

presented in Table 4. The resistance profile of the clinical isolates can be found in Supporting Information S2: Table S1.

In Series-1 (1–17) containing the extended urea linker, no substantial antimycobacterial activity was registered. Low solubility in DMSO (stock solutions) limited the highest concentrations of some compounds that were achieved. Compounds 11 and 14 bearing 2-Cl and 2-Br substitution, respectively, were highly insoluble in DMSO

and could not be evaluated. From Series-1, only compound 5 containing *tert*-butyl moiety at *para* position of the phenyl ring exhibited an isolated mild activity against *M. kansasii* with MIC = 62.5 µg/mL.

As the apparent lack of antimicrobial activity introduced by the minute structural modification of the linker was unexpected, we decided to investigate the potential reasons further. The 1D-nuclear overhauser effect spectroscopy (NOESY) and in silico explorations of low-energy conformations of the Series-1 prototypical compound 1 concluded that the synthesized ureas are, in fact, geometrically different from the previously described

amides.<sup>[10]</sup> This is due to the formation of an intramolecular H-bond (IMHB) between urea linker -NH- and the N4 of the pyrazine ring, fixing the molecule in the *cis-trans* conformation and promoting different arrangement of the important structural features. Therefore, next to the low solubility of urea derivatives, their inactivity is most probably linked to the incompatibility of this conformation with the shape of the mtProRS active site. More specifically, only the energetically less favorable *trans-trans* conformer of compound 1 can adopt the probable binding mode of amidic derivatives from Generation 1,<sup>[10]</sup> that is, to occupy the ribose binding site by the phenyl substituent (Figure 3).

The Series-2 (18–24) compounds with the amidic linker and 4-substituted or 2,4-disubstituted benzamide core exhibited very interesting results, as shown in Table 2. In our earlier study, we observed that the 4-substitution proved to be important for the activity against *Mtb* (and predicted binding to the adenosine binding site of mtProRS),<sup>[10]</sup> while the 2-substitution was important for binding to hsProRS but lacked the inhibitory activity against *Mtb*.<sup>[9]</sup> Compounds 21 and 22 containing 4-Cl or 4-Br (respectively) and 2-F retained moderate activity against *Mtb* H37Ra with MIC 31.25 µg/mL. This activity retention can be explained by comparable sizes of the 2-F substituent and hydrogen atom (as in the previously reported 2-unsubstituted derivatives). Both compounds exhibited activities against all mycobacterial species with excellent activity against *M. kansasii* with MIC = 3.91 µg/mL and showed promising results also against the virulent strain *Mtb* H37Rv or the MDR clinical isolates, with compound 22 showing slightly better activity. No antimycobacterial activity was observed in disubstituted compounds of Series-2 bearing 2-substituent larger than fluorine (19, 23, 24). On the opposite, position 4 requires a sterically larger substituent, 4-F in 20 and 23 led to inactive compounds. The observed SAR are in agreement with our previous studies. Based on the presented results, we can further expand and confirm the already known SAR by stating

**TABLE 4** The results of antimycobacterial screening of selected compounds against virulent *Mtb* H37Rv and the MDR strains.

Code	MIC (µg/mL)			
	<i>Mtb</i> H37Rv	<i>Mtb</i> SORO	<i>Mtb</i> IZAK	<i>Mtb</i> MATI
19	>100	>100	>100	>100
20	>100	>100	>100	>100
21	12.5	25	25	25
22	6.25	12.5	12.5	12.5
23	>100	>100	>100	>100
24	>100	>100	>100	>100
25	>100	>100	>100	>100
26	>100	>100	>100	>100
27	>100	>100	>100	>100
29	100	100	100	100
INH	0.2	>100	>100	>100

Abbreviations: INH, isoniazid; MDR, multidrug-resistant; MIC, minimum inhibitory concentration.

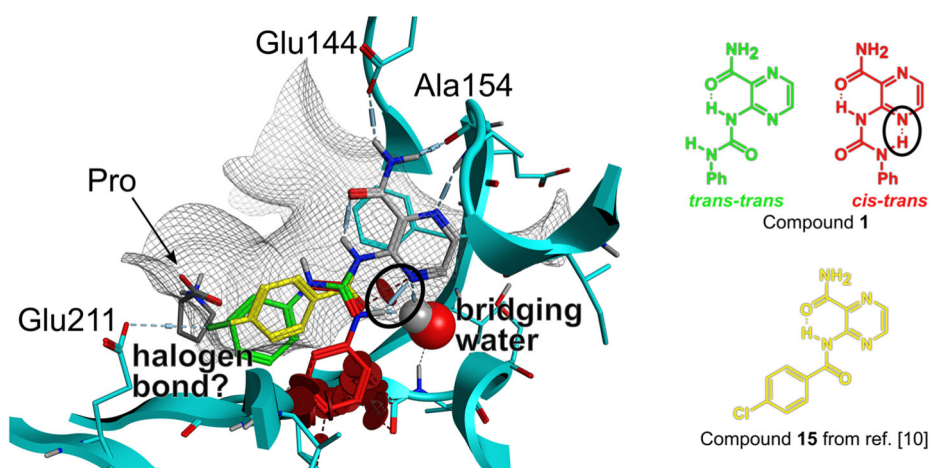


**FIGURE 3** Overlay of urea 1 in *cis-trans* (red carbons) and *trans-trans* (green carbons) conformation with probable binding mode of compound 15 from published work<sup>[10]</sup> (yellow carbons) in the active site of mycobacterial prolyl-transfer RNA synthetase. The visualized surface corresponds to the van der Waals interaction surface of the binding site. Red cylinders around the phenyl ring represent a steric clash of *cis-trans* conformer with the protein. The black ellipse highlights the discussed intramolecular H-bond.

that in position 2, it is mostly steric effects that play a key role in the activity, while the 4-substituent is best kept as small alkyl or a halogen larger than fluorine.

The previous generation of the cyclized derivatives containing pteridin-4(3H)-one moiety exhibited moderate activities with MIC = 31.25–62.5 µg/mL against *Mtb* H37Ra.<sup>[10]</sup> Series-3, that is 4H-pyrazino[2,3-d][1,3]oxazin-4-ones (further referred to as pyrazinooxazinones, **25–29**), represent *O*-isosteres (lactones) of the formerly mentioned pteridines. Compounds **25**, **27**, **28**, and **29** were previously reported but not considered or tested for antimicrobial activity.<sup>[14,15]</sup> The pyrazinooxazinones were tested against all strains of *Mtb*, including MDR strains, but possessed no activity. However, since the synthesized compounds are lactones, the cyclic esters that are prone to ring openings by chemical hydrolysis or metabolism, they can be considered as prodrugs of 3-benzamidopyrazine-2-carboxylic acids structurally related to the confirmed inhibitors of mycobacterial aspartate decarboxylase (PanD).<sup>[16]</sup> To verify this concept, we evaluated the stability of compound **29** as a representative of Series-3 (see Section 2.4).

## 2.4 | Assessment of the stability and in vitro human liver microsomes (HLM) metabolism of compound 29

The chemical stability of lactone **29** was studied under various conditions by HPLC-HRMS. First, we assessed the immediate chemical stability in various mixtures of solvents. These samples were measured without any delay. In this setup, the lactone **29** was stable in DMSO/water (50:50) and DMSO/MeCN (50:50) mixtures but completely hydrolyzed to the opened form in a 50:50 mixture of DMSO with incubation buffer (0.1 M potassium phosphate buffer, pH 7.4). In pure MeOH, the parent compound underwent transesterification by MeOH. The immediate measurement showed 57% of the remaining parent

compound **29** and 43% of the methyl ester product (confirmed by HPLC-HRMS analysis of chemical standard). After 72 h in MeOH, there was only 4% of parent **29** remaining. The chromatograms are shown in Supporting Information S2: Figure S1.

Despite the chemical instability of lactone **29** in the incubation buffer, we attempted to identify further metabolites upon incubation with HLM. Besides the obvious opened form, which was already present in the chemical control (incubation only in the presence of buffer without HLM), a metabolite with additional hydroxylation was detected by HRMS (Supporting Information S2: Figure S2). In the control experiment, the HLM biotransformation was performed for the lactam predecessor of compound **29** (a sample from our previous study),<sup>[10]</sup> for which no significant metabolites were found. Figure 4 summarizes the stability and metabolization of lactone **29**.

## 2.5 | Determination of the three-dimensional (3D) structure of selected prototypical urea derivative

Generally, substituted ureas can exist in four main conformations, classified by the relative orientation of the large substituents at *N* and *N'* (*trans-trans*, *cis-trans*, *trans-cis*, or *cis-cis*).<sup>[17]</sup> The *trans-trans* conformers are generally prevalent, but the compound-specific conformation depends on the substitution pattern, which is based mainly on the steric properties and noncovalent interaction potential of the substituents.<sup>[18,19]</sup> In theory, our urea derivatives (Series-1) can take four distinct conformations of the urea linker (Figure 5). In contrast with the general preference for *trans-trans* conformers, we hypothesized that the energetically lowest conformer of urea derivatives from Series-1 could be *cis-trans* because of the additional stabilization of this conformer by IMHB between the distal urea hydrogen and N4 of the pyrazine core.

The low-energy conformation of the prototype urea derivative **1** was studied to understand potential reasons for the lack of

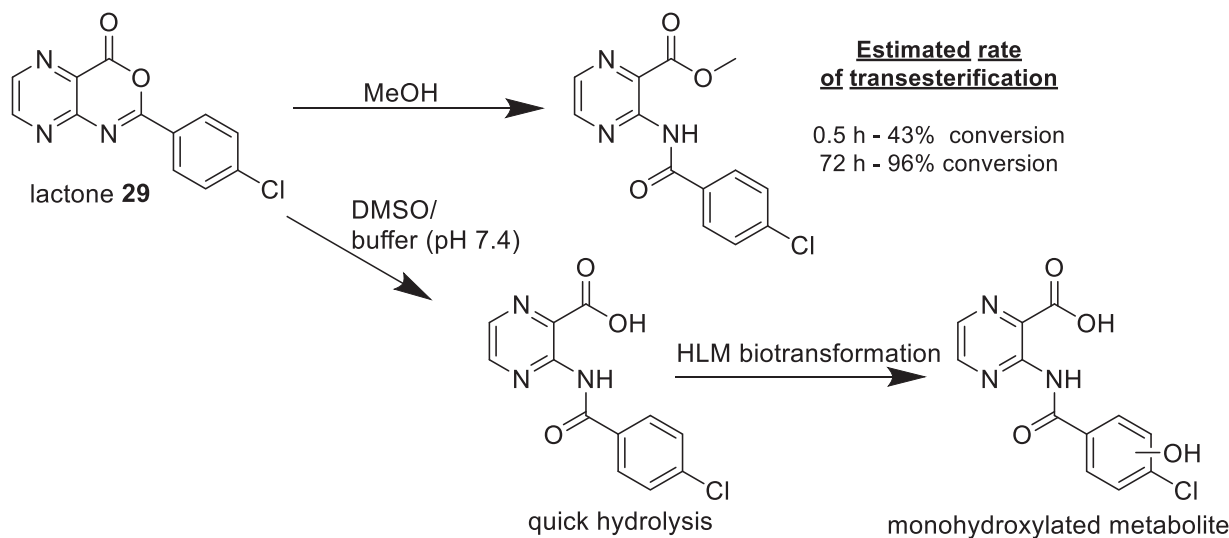


**FIGURE 4** Overview of solvent stability and human liver microsomes metabolism of lactone **29**.



antimicrobial activity when comparing the ureas to previously synthesized amides (first generation). The conformation of **1** was studied computationally by comparison with related experimental structures in the Cambridge Structural Database (CSD) and finally by a 1D-NOESY experiment.

### 2.5.1 | In silico prediction of the 3D structure of urea derivative **1**

The relaxed dihedral scan of both torsion angles (at B3LYP/def2-SVP level of theory, Figure 6) indicated a clear energetic preference for the *cis-trans* isomer, followed by *trans-trans* isomer and *trans-cis*

isomer. The *cis-cis* hypothetical isomer was unrealistic due to a significant distortion of the structure.

The *cis-trans* and *trans-trans* isomers were considered further and studied in the bidirectional relaxed scan of the DIH1 angle at the same level of theory but in the implicit solvent model of water (SMD variation of integral equation formalism polarisable continuum model (IEFPCM)).<sup>[20]</sup> This scan allowed us to estimate the rotation barrier around the DIH1 angle, defined as the energy difference between the *cis-trans* isomer and the estimated transition state (TS, DIH1 = 98°). The rotation barrier was estimated to be 9.72 kcal/mol (B3LYP/def2-SVP, implicit water, Figure 7).

The low-lying *cis-trans* and *trans-trans* conformers were further optimized at a higher level of theory (B3LYP/def2-TZVP, implicit

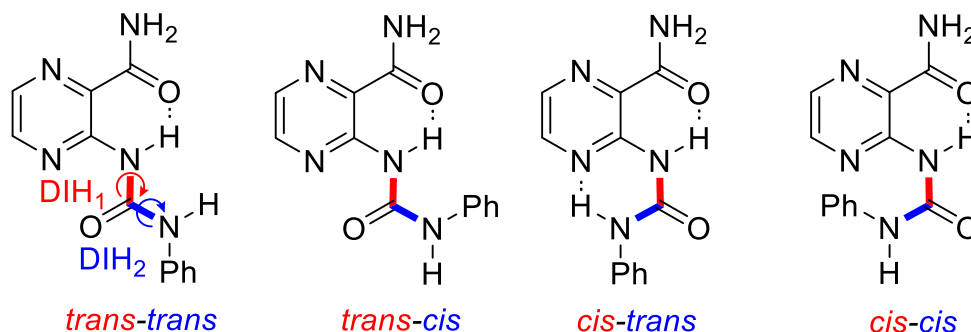


**FIGURE 5** Possible conformations of urea derivatives (Series-1) with respect to the urea linker.

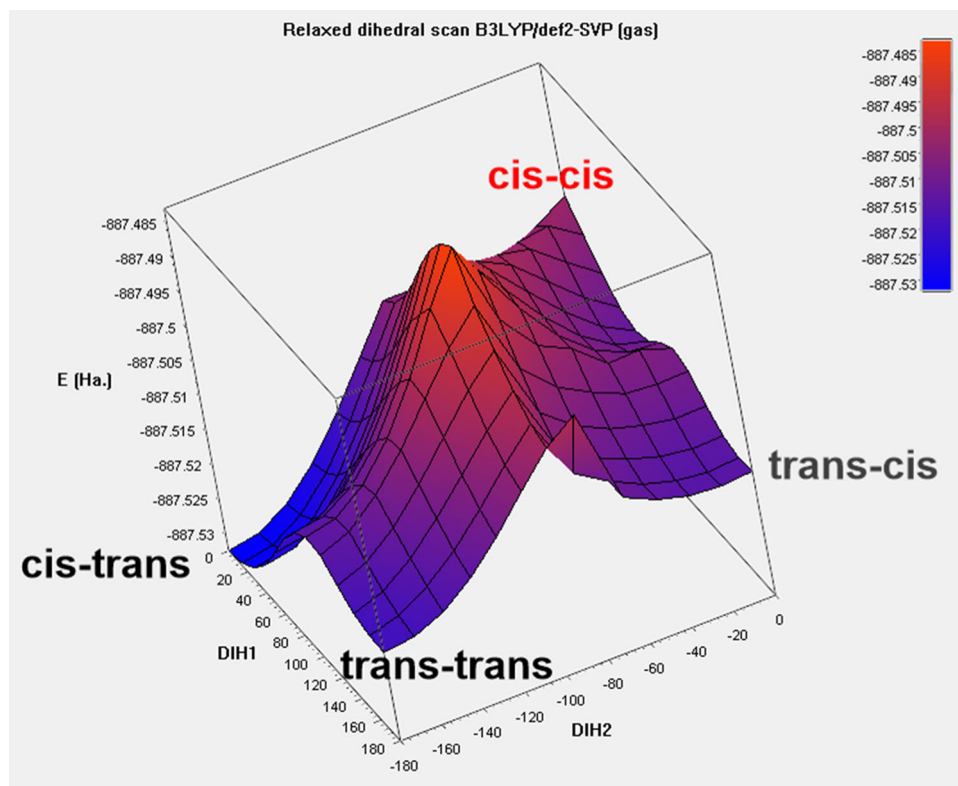


**FIGURE 6** Potential energy surface of compound **1** with respect to the conformation of the urea linker, calculated in the gas phase at B3LYP/def2-SVP level of theory.

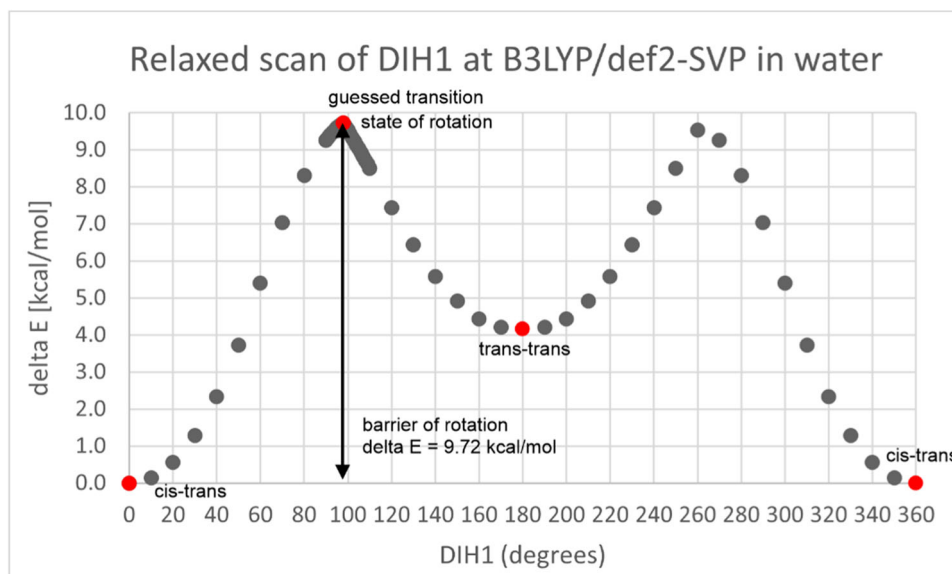


**FIGURE 7** Relaxed dihedral scan of DIH1 calculated in implicit water at B3LYP/def2-SVP level of theory (points indicate the energetically lower conformer of the clockwise and counterclockwise scan). Red points indicate conformers of interest.

water). In this model of chemistry, the energy difference between the *trans-trans* conformer and *cis-trans* conformer was 3.07 kcal/mol. Converted to Boltzmann factors ( $p = \exp(\Delta E/kT)$ , where  $k$  is the Boltzmann constant,  $T$  is the absolute temperature 278.15 K, and  $\Delta E$  is the energy difference between the conformers expressed in J per one molecule), the relative abundance of the wanted *trans-trans* conformer is 0.56%. The Cartesian coordinates of the optimized structures can be found in the Supplementary Material. In summary, the computational predictions determined the *cis-trans* isomer to be the dominant species of the conformation ensemble. The estimated barrier of rotation of DIH1 (9.72 kcal/mol at B3LYP/def2-TZVP) is consistent with previously reported calculations (B3LYP/DZVP2) for various monosubstituted ureas (9.66–9.68 kcal/mol).<sup>[18]</sup>

### 2.5.2 | NOESY NMR of compound 1

The conformation arrangement of urea derivative **1** in solution was evaluated by nuclear overhauser effect (NOE) experiments. There was an obvious correlation of the hydrogen of the NH-phenylurea group (chemical shift  $\delta$  11.22 ppm) with the hydrogen of the phenyl ring at position 2 ( $d = 7.61$  ppm) and with the hydrogen of the pyrazine ring at position 5 ( $\delta$  8.60 ppm). The latter correlation confirmed the spatial proximity of the urea linker hydrogen with pyrazine hydrogen (H5), indicating the *cis-trans* conformation stabilized by nonbonding interactions (Figure 8, left panel). The obtained 1D-NOESY spectrum is presented in Supporting Information S2.

### 2.5.3 | CSD analysis

The distribution of the urea linker dihedral angles in crystallographic experimental structures was obtained by querying the Cambridge

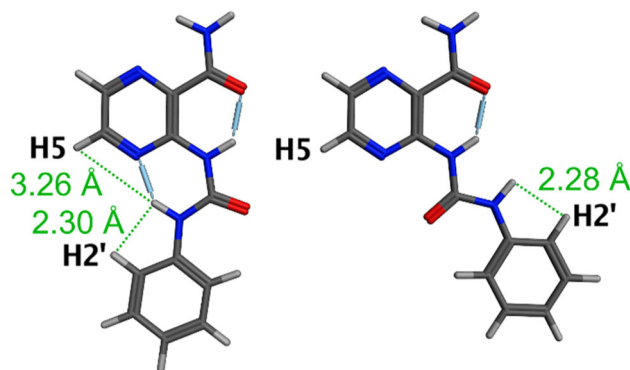


**FIGURE 8** Selected interproton distances of *cis-trans* and *trans-trans* conformers of urea derivative **1** (mmff94x optimized structures).

Structural Database (CSD) version 5.44. The database was queried for ureas with phenyl and hydrogen on one nitrogen atom and with a nitrogen-containing heterocycle (endocyclic nitrogen atom must be in *ortho* position to the linker) and a hydrogen atom on the other urea nitrogen (Figure 9a). Dihedral angles DIH1 (Cpyr-N-C-N) and DIH2 (N-C-N-Car) as indicated in Figure 9a were gathered and statistically evaluated.

In total, the CSD search yielded 66 datapoints representing 46 unique molecules. No pyrazine-containing compounds were found; we identified only fragments of pyridine or pyrimidine (free or in condensed heterocycles). However, since N1 of the pyrazine core (numbered in agreement with the numbering of compound **1**) is not expected to be involved in any intramolecular interactions with the urea linker and thus have little to no effect on the final conformation, the obtained pyridine- and pyrimidine-based structures are relevant for the general conformational trend of our studied

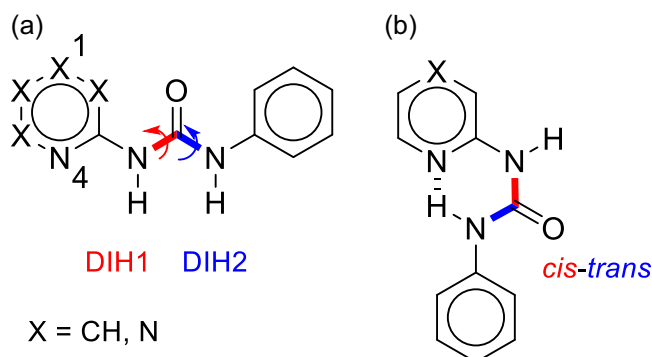


**FIGURE 9** (a) Definition of the Cambridge Structural Database search query; (b) depiction of the dominant conformation *cis-trans*.

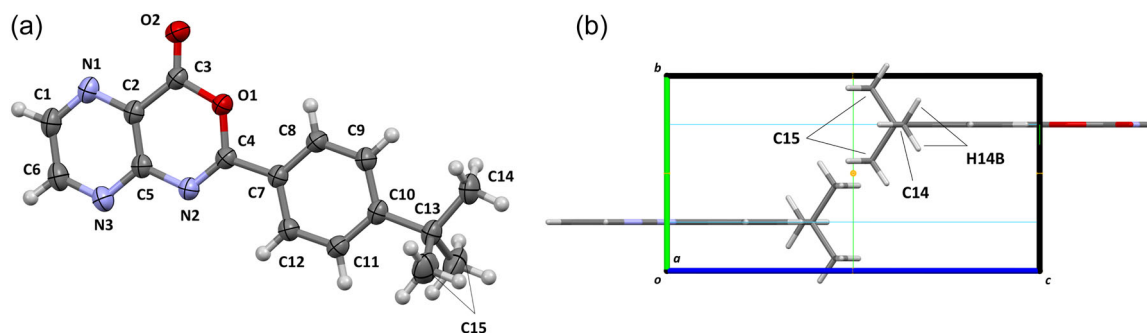


**FIGURE 10** (a) Thermal ellipsoid diagram of **26**, with the arbitrary atom-numbering scheme. Displacement ellipsoids are drawn at the 40% probability level. (b) Representation of the unit cell viewed along the *a* axis. The  $P2_1/m$  symmetry operators are drawn as follows: inversion center—orange dot; twofold axis—green line; mirror plane: light-blue line.

urea derivatives. For statistical analysis, compounds substituted on N4 and pyridinium salts were excluded, leaving 46 datapoints representing 31 unique molecules. As expected, and in accordance with the quantum mechanics calculations and NOESY experiment, the dihedral angles in the analyzed compounds were tightly distributed around the *cis-trans* conformation (Figure 9b), stabilized by the IMHB. For DIH1, the mean value was  $3.3^\circ$  ( $0.0\text{--}10.7^\circ$ ) while the DIH2 reached  $176.0^\circ$  ( $168.3^\circ\text{--}180.0^\circ$ ). These results confirm the significant influence of the IMHB on the stabilization of the low-energy conformations of the related heteroaromatic-substituted ureas.

Only one CSD entry deviated from this conformational trend, CSD ID: PIWVEZ (two datapoints). In this derivative, both aromatic cores forming the ureide were further substituted with longer linear side chains and *trans-trans* conformation seemed more preferred (in reported crystals). The average values of DIH1 and DIH2 were  $176.4^\circ$  and  $173.1^\circ$ , respectively, indicating the *trans-trans* conformation.

## 2.6 | Crystallography of compound **26**

Compound **26** was analyzed by single-crystal X-ray diffraction to ascertain the formation of the pyrazinooxazinone ring and study the 3D arrangement of this new class of compounds. The unit-cell

determination revealed a monoclinic  $P2_1/m$  system. The thermal ellipsoid diagram, indicating the arbitrary atom-numbering scheme used in the discussion, is reported in Figure 10a. The molecule lies on the mirror plane so that two of the methyl groups (C15) of the *tert*-butyl moiety and two hydrogens of the other methyl (C14) are related by crystallographic mirror symmetry (Figure 10b). As a result, the asymmetric unit shows only two methyl groups, one of which (C14) with only two hydrogen atoms.

The overall structure is planar, with C14 of the *tert*-butyl group lying on the same plane of the aromatic rings and the other methyl groups organized in a standard tetrahedral geometry. The C3–O2 bond of the lactone is slightly bent, forming an angle of  $117.5(1)^\circ$ , calculated on the O1–C3–O2 triad. All bond lengths, valence angles, and torsional angles are within the expected limits for similar compounds, as shown by CSD Mogul.<sup>[21,22]</sup> In the crystal, the molecules are connected by H-bonds between  $\text{C}\pi\text{H8-N3}$ ,  $\text{C}\pi\text{H6-O2}$ , and  $\text{C}\pi\text{H6-O1}$  (weak), forming planar chains extending along the *a* axis. Weak van der Waals interactions are established by the *tert*-butyl groups, joining the chains along the *b*-axis. The packing and the main interactions are visualized in Figure 11; a full account of the H-bonds is available in Table 5.

The intermolecular contacts were further characterized by the analysis of the Hirshfeld surface (HS) mapped over the normalized contact distance ( $d_{\text{norm}}$ ).<sup>[23]</sup> The  $d_{\text{norm}}$  property (Figure 12a) was

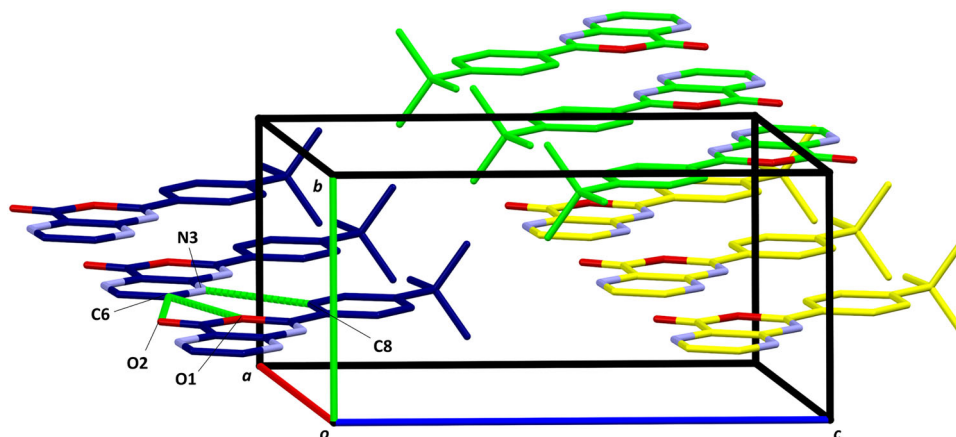


**FIGURE 11** Stick model of compound **26** showing the main H-bonds, in an arbitrary view. Molecules on different planes are colored differently. Hydrogens are omitted for clarity.

**TABLE 5** H-bond geometry (D: donor, A: acceptor).

	D-H/Å	H...A/Å	D...A/Å	D-H...A/°
C8-H8...N3 <sup>I</sup>	0.930(2)	2.587(2)	3.420(2)	149.3(1)
C6-H6...O1 <sup>III</sup> , <sup>IV</sup>	0.930(2)	2.764(1)	3.624(2)	154.2(1)
C6-H6...O2 <sup>III</sup> , <sup>IV</sup>	0.930(2)	2.555(1)	3.430(2)	157.0(1)

Note: Equivalent positions: <sup>I</sup> $x + 1, y, z$ ; <sup>II</sup> $x + 1, 1/2 - y, z$ ; <sup>III</sup> $x - 1, y, z$ ; <sup>IV</sup> $x - 1, 1/2 - y, z$ .

visualized with a red-blue-white color scheme, based on the length of the intermolecular contacts with respect to the sum of the van der Waals radii. The analysis of the surface revealed a prevalence of blue-to-white areas; red spots, indicating shorter-range contacts, appeared in correspondence to the H-bonds and the van der Waals interactions (fainter spots). The two-dimensional (2D) fingerprint of the HS (Figure 12b), providing a visual summary of the contribution of each contact type and the relative area of the surface corresponding to it, was characterized by a compact shape, without significant spikes, confirming the absence of short-range intermolecular contacts.

### 3 | CONCLUSION

In conclusion, this study presents a comprehensive exploration of three series of distinct compounds designed as structural expansions of previously identified antimycobacterial agents targeting ProRS. In total, we describe the preparation and characterization of 29 compounds containing urea (Series-1), carboxamide linker (Series-2), or lactone-type derivatives of 4H-pyrazino[2,3-d][1,3]oxazin-4-ones (Series-3). Evaluation of antimycobacterial activity revealed diverse outcomes: while urea derivatives showed limited activity and poor solubility, amidic derivatives exhibited promising antimycobacterial effects, particularly with specific halogen substituents. Computational investigations provided further insights into the preferred conformations of urea derivatives, thus explaining the lack of antimycobacterial activity as a result of shape-based conformational incompatibility of the substituted urea linker with the

ProRS active site. The low-energy conformer was also confirmed experimentally by NOESY experiments. Finally, although the lactone derivatives displayed no antimycobacterial activity, their metabolic stability evaluation revealed their potential as prodrugs of next-generation PanD inhibitors derived from 3-aminopyrazine-2-carboxylic acid. This would, however, require further optimization of the kinetics of their hydrolysis. Overall, this study contributed valuable SAR data to the development of novel antimycobacterial agents targeting ProRS and potentially PanD, paving the way for future optimization and drug discovery efforts.

## 4 | EXPERIMENTAL

### 4.1 | General

All chemicals (unless stated otherwise) were purchased from Merck and Fluorochem. The reaction progress was monitored using Merck Silica 60 F<sub>254</sub> thin layer chromatography (TLC) plates (Merck). MW-assisted reactions were performed in a CEM Discover MW reactor (CEM Corporation) with a focused field connected to Explorer 24 autosampler (CEM Corporation), and the equipment was running under CEM Synergy™ software for setting and monitoring reaction conditions. The temperature of the reaction mixture was monitored by an internal infrared sensor. Purification of synthesized compounds was performed on automated flash chromatograph puriFlash XS420+ (Interchim) using original columns (spherical silica, 30 μm). The mixture of EtOAc and hexane (Hex) was used as a mobile phase with an elution gradient of 0%–100% EtOAc in Hex. Detection was performed by a UV-VIS detector at wavelengths of 254 and 280 nm. NMR spectra were recorded on Varian VNMR S500 (Varian) at 500 MHz for <sup>1</sup>H and 125 MHz for <sup>13</sup>C or using Jeol JNM-ECG600 at 600 MHz for <sup>1</sup>H and 151 MHz for <sup>13</sup>C. All spectra were recorded in DMSO-*d*<sub>6</sub>; compound **25** was recorded in CDCl<sub>3</sub>. The chemical shifts given as δ values in ppm were indirectly referenced to tetramethylsilane via the solvent signal (2.49 ppm for <sup>1</sup>H and 39.7 ppm for <sup>13</sup>C in

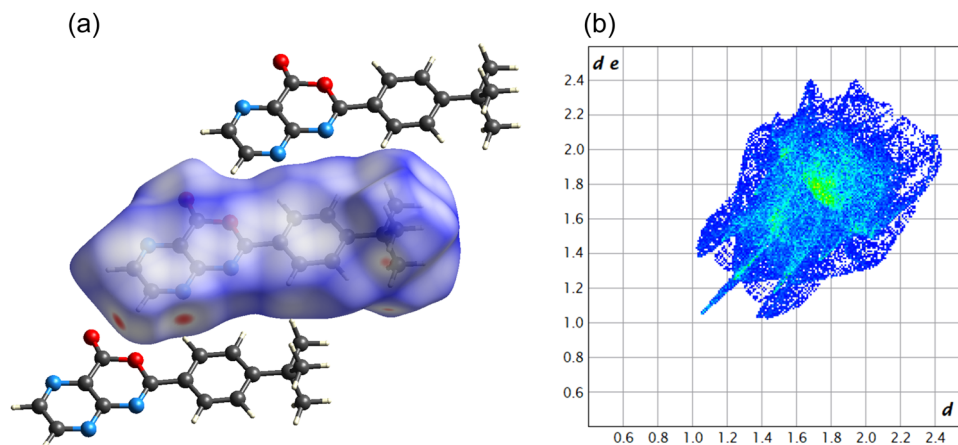


**FIGURE 12** (a) Hirshfeld surface (HS) mapped over  $d_{norm}$  with a fixed color scale in the range  $-0.1431$  au (red)  $-1.2584$  au (blue), based on the length of the intermolecular contacts with respect to the sum of the van der Waals radii (red: shorter; blue: longer; white: same). (b) Two-dimensional fingerprint plot of the HS of **26**. The graphical representation provides a summary of the frequency of each combination of  $d_e$  (distances from the HS to the nearest nucleus outside the surface) and  $d_i$  (distances from the HS to the nearest nucleus inside the surface) across the HS. Points with a lower contribution to the surface are colored blue, while green indicates larger contributions.

DMSO- $d_6$  and 7.26 for  $^1\text{H}$  and 77.16 for  $^{13}\text{C}$  in  $\text{CDCl}_3$ ). Nicolet 6700 spectrometer (Thermo Scientific) was used to measure IR spectra using the ATR-Ge method. The purity of the final compounds was checked by an elemental analysis performed on the Vario MICRO cube Element Analyzer (Elementar Analysensysteme). CLog  $P$  values were calculated using ChemDraw v22.2.0. (PerkinElmer Informatics). Melting points of the synthesized compounds were measured in an open capillary on the Stuart SMP30 melting point apparatus (Bibby Scientific Limited) and were uncorrected.

The purity of final compounds containing fluorine was assessed by HPLC measurement using a Shimadzu LC20 chromatograph (Shimadzu) coupled with a PDA detector (SPD-M20A) on the column ZORBAX ECLIPSE XDB- $\text{C}_{18}$  ( $3.0 \times 50$  mm,  $1.8 \mu\text{m}$ , Agilent Technologies) using acetonitrile/water mobile phase mixture in gradient mode. Data were processed using LabSolutions software (v. 5.92, Shimadzu). The stock solution of each compound ( $1.0$  mg/mL) was prepared by dissolving the appropriate amount in methanol. Working solutions were prepared by diluting the stock solutions with the acetonitrile/water mixture (1:1, v/v) to a concentration of  $50 \mu\text{g/mL}$ . The PDA detector acquired spectra from 210 to 800 nm and wavelengths of 260 and 363 nm were employed for purity evaluation.

## 4.2 | Chemistry

### 4.2.1 | Synthesis of intermediate compounds (I–V)

3-Chloropyrazine-2-carbonitrile (**I**): Obtained from Fluorochem and used without further purification.

3-Chloropyrazine-2-carboxamide (**II**): In a 100 mL round-bottom flask (RBF), the mixture of 2.9 mL conc. hydrogen peroxide (30% v/v), and 19.5 mL of distilled water were heated to  $50^\circ\text{C}$  and alkalinized to

pH 8–9 using an 8% m/m sodium hydroxide solution. The mixture was stirred and charged with 10.0 mmol of 3-chloropyrazine-2-carbonitrile (**I**) added in small portions over a period of 0.5 h while maintaining the basic pH of 8.0–9.0. The reaction was continued for 2.5 h at  $55^\circ\text{C}$ . Yellow crystals of crude product were observed in the reaction mixture. The mixture was cooled, and the crude product was filtered under reduced pressure and washed with cold water. The crude product was recrystallized from hot ethanol to obtain a white crystalline product in sufficient purity for further reactions. White crystalline. Yield: 60%. Mp  $187.0$ – $188.8^\circ\text{C}$  ( $187.1$ – $189.2^\circ\text{C}$  in literature (lit.)<sup>[24]</sup>).  $^1\text{H}$  NMR (600 MHz, DMSO- $d_6$ )  $\delta$  8.68 (d,  $J = 2.5$  Hz, 1H, PzH), 8.62 (d,  $J = 2.5$  Hz, 1H, PzH), 8.18 (s, 1H, CONH), 7.93 (s, 1H, CONH).

3-Aminopyrazine-2-carboxamide (**III**): Into a 10 mL MW tube containing 1.0 mmol of 3-chloropyrazine-2-carboxamide (**II**), 5 mL (excess) of 7 N ammonia in anhyd. methanol (Merck) was added. The sealed reaction was conducted in the MW reactor ( $120^\circ\text{C}$ , power limit 120 W, pressure limit 120 psi). After 0.5 h, the reaction was checked by TLC, and if the starting material **II** was still visible, the reaction time was extended to 0.75 h in total. Once the reaction was completed, the excess ammonia in methanol was evaporated under reduced pressure, and a white precipitate of **III** was obtained and used for further reactions without any additional purification steps. White Solid. Yield: >95%. mp  $240.1$ – $241.7^\circ\text{C}$  ( $238.4$ – $239.4^\circ\text{C}$  in lit.)<sup>[25]</sup>.  $^1\text{H}$  NMR (600 MHz, DMSO- $d_6$ )  $\delta$  8.18 (d,  $J = 2.4$  Hz, 1H, PzH), 8.06 (s, 1H, CONH), 7.80 (d,  $J = 2.4$  Hz, 1H, PzH), 7.58 (s, 1H, CONH).

Methyl 3-aminopyrazine-2-carboxylate (**IV**): Obtained from Fluorochem and purified in automated flash chromatography using gradient mobile phase of Hex/EtOAc 0%–70%. A pale yellow product is retrieved after purification, which seems to exhibit higher reactivity compared to brown-colored unpurified **IV** starting material.

The key intermediates, methyl 3-benzamidopyrazine-2-carboxylates (**V**), were prepared as previously reported.<sup>[10]</sup>

## 4.2.2 | Synthesis of the final compounds

3-Ureidopyrazine-2-carboxamide derivatives (**1–17**; Series-1): A 10 mL MW tube containing 1.0 mmol of 3-aminopyrazine-2-carboxamide (**III**) in 3–4 mL of MeCN was charged with 3.0 mmol of the corresponding substituted phenyl isocyanate (Merck). The reaction was conducted in a pressurized MW reactor at 120°C for 0.5 h, using 120 W power and a safety pressure limit of 120 psi. After cooling, the crude products precipitated and were filtered under reduced pressure. Since most of the products were of low solubility in many solvents, they were repeatedly washed with water and other organic solvents such as hexane, dichloromethane, and acetone. Finally, the obtained products were purified using a precipitation technique—partial dissolution in hot acetone, followed by precipitation induced by the addition of cold hexane. The products were isolated as solids in yields ranging between 20% and 30%.

3-Benzamidopyrazine-2-carboxamide derivatives (**18–24**; Series-2): In a 50 mL RBF containing 1.0 mmol of 3-aminopyrazine-2-carboxamide (**III**), 15 mL of anhyd. MeCN was added, followed by 2.6 mmol of anhyd. pyridine and stirred under ambient temperature for 5 min. Further, 2.1 mmol of the corresponding substituted benzoyl chloride (Merck) was added dropwise into the reaction mixture, followed by heating the reaction mixture to 50°C with stirring for 24 h. Once the reaction was completed, the solvents were evaporated under reduced pressure, and the crude product was purified using automated flash chromatography on silica using gradient elution by 0%–100% EtOAc in Hex. The final products were isolated as solids with 70%–80% yields.

Pyrazinooxazinone derivatives (**25–29**; Series-3): In a 50 mL RBF, 1.0 mmol of the corresponding methyl 3-benzamidopyrazine-2-carboxylate (prepared according to our previous paper<sup>[10]</sup>) was mixed with 15 mL of anhyd. toluene, followed by 1.1 mmol of triphenylphosphine and 3.0 mmol of triethylamine. After stirring the reaction mixture for 0.25 h at 80°C, 1.1 mmol of 1,2-dibromotetrachloroethane was dissolved in anhyd. toluene and added dropwise. The reaction continued from 4 to 6 h at 80°C while monitoring the reaction progress on TLC. Once the reaction was completed, the hot reaction mixture was immediately filtered to remove precipitated triethylammonium chloride, followed by evaporating solvents under reduced pressure. The crude product was washed with ethanol and recrystallized using MeCN. The products were isolated as solids in 10%–30% yields.

The InChI codes of the investigated compounds, together with biological activity data, are provided as Supporting Information [S1](#).

## 4.3 | In vitro antimycobacterial evaluation

The in vitro antimycobacterial activity was assessed using a microdilution broth method based on a Microplate Alamar Blue Assay (MABA).<sup>[10]</sup> The results were expressed as a MIC in µg/mL. For methodology and characterization of the used strains; see Supporting Information [S2](#).

## 4.4 | Crystallographic studies

Crystals of **26** were obtained at room temperature as colorless plates by the slow evaporation of a MeCN solution. X-ray intensity data were collected at 298.45(10) K with a Rigaku XtaLAB Synergy Dualflex diffractometer (Rigaku), equipped with a microfocus PhotonJet Cu-K $\alpha$  source and a Hybrid Pixel Array Detector. Data collection was performed with omega scans with a step size of 0.5° and an exposure time of 90 s/frame. A total of 7806 Bragg reflections were collected, giving a metrically monoclinic unit; the analysis of the systematic absences indicated the space group P2<sub>1</sub>/m. Intensity data were integrated and empirically corrected for Lorentz-polarization effects, using the Rigaku CrysAlisPro 1.171.42.101a software (Rigaku Oxford Diffraction/Agilent Technologies UK Ltd.). The structure was solved by direct methods using SIR2019/3<sup>[26]</sup> and completed by iterative cycles of full-matrix least-squares refinement on  $F_o^2$  and  $\Delta F$  synthesis using SHELXL-2019/3<sup>[27]</sup> within the WinGX suite (WinGX v.2021.3).<sup>[28]</sup> Hydrogen atoms were introduced at calculated positions in their described geometries and allowed to ride on the attached atom with fixed isotropic thermal parameters (1.2 and 1.5 U<sub>eq</sub> of the parent atom for aromatic and methyl, respectively). The hydrogens connected to C14 (H14A and H14B) were located on the Fourier difference map to avoid artifacts due to the mirror symmetry. Moreover, all atoms lying on the mirror plane were automatically assigned an occupancy of 0.5. The structure was analyzed with PARST,<sup>[29]</sup> and the graphical representations were rendered with Mercury 2022.3.0.<sup>[30]</sup> HS analysis was performed with CrystalExplorer21.<sup>[31]</sup>

*Crystal data for 26*: Formula: C<sub>16</sub>H<sub>15</sub>N<sub>3</sub>O<sub>2</sub> (full), C<sub>8</sub>H<sub>7.5</sub>N<sub>1.5</sub>O (asymmetric unit); MW: 281.31 g/mol (full), 140.65 g/mol (asymmetric unit); Temperature: 298.45(10) K; Wavelength: 1.54184 Å; Bravais lattice: monoclinic; Space group: P2<sub>1</sub>/m; Unit cell dimensions:  $a = 8.0897(3)$  Å,  $b = 6.7561(2)$  Å,  $c = 13.2851(4)$  Å,  $\beta = 103.654(3)^\circ$ ;  $V = 705.57(4)$  Å<sup>3</sup>;  $Z = 4$ ;  $D_{\text{calc}} = 1.324$  Mg/m<sup>3</sup>; Absorption coefficient: 0.730 mm<sup>-1</sup>;  $F(000) = 296$ ; Crystal size: 0.30 × 0.12 × 0.05 mm;  $2\theta_{\text{min}} = 3.424^\circ$ ;  $2\theta_{\text{max}} = 70.026^\circ$ ; Limiting indices =  $-9 \leq h \leq 9$ ,  $-8 \leq k \leq 8$ ,  $-16 \leq l \leq 13$ ; Collected reflections: 7806; Independent reflections: 1463 ( $R_{\text{int}} = 0.0208$ ); Completeness to 67.684°: 100.0%; Refinement method: Full-matrix least-squares on  $F^2$ ; Data/restraints/parameters: 1463/0/129; GOOF: 1.070; Final R indices [ $I > 2\sigma(I)$ ]:  $R1 = 0.0376$ ,  $wR2 = 0.1067$ ; R indices (all data):  $R1 = 0.0420$ ,  $wR2 = 0.1110$ ; Largest diff. peak and hole: 0.128 and  $-0.174$  e Å<sup>-3</sup>. Cambridge Crystallographic Data Centre deposition number: 2306232.

*HS data for 26*: Volume: 346.34 Å<sup>3</sup>; Area: 317.07 Å<sup>2</sup>; Globularity (G): 0.752; Asphericity ( $\Omega$ ): 0.379.

## 4.5 | In silico methods

### 4.5.1 | Force field calculations

Force field calculations were performed in Molecular Operating Environment 2022.02 (Chemical Computing Group ULC) under Amber10:EHT force field if not otherwise stated.

## 4.5.2 | Electronic structure calculations

The calculations were performed in Gaussian 16 rev. C.01 (Gaussian Inc.)<sup>[32]</sup> and run on clusters of MetaCentrum (MetaVO). Visualization was carried out using GaussView 6.1.1 (Semichem Inc., Shawnee Mission, 2016).

The initial relaxed dihedral 2D scan (Figure 6) was done using B3LYP/def2-SVP level of theory. The dihedral angles DIH1 (defined as  $N_{\text{urea}}-C_{\text{urea}}-N_{\text{urea}}-C_{\text{pyrazine}}$ ) and DIH2 (defined as  $N_{\text{urea}}-C_{\text{urea}}-N_{\text{urea}}-C_{\text{Ph}}$ ) were changed in 15° increments starting from the *cis-trans* isomer (DIH1 = 0°, DIH2 = -180°). All other parameters were subject to structure optimization.

The following bidirectional relaxed scan of DIH1 (Figure 7, corresponding to *cis-trans* to *trans-trans* conformational change) was performed using the same theory but including the implicit solvent model of water (SMD variation of IEFPCM).<sup>[20]</sup> Starting from the *cis-trans* conformer optimized in the previous step, the DIH1 has generally changed in 10° increments and subsequently in 1° increments around the first local maximum (expected TS). All other parameters were subject to structure optimization. The scan was performed both clockwise and counterclockwise, and the lowest conformer from both scans was depicted.

Conformers of interest (*cis-trans*, *trans-trans*) were then reoptimized on a higher theory using B3LYP/def2-TZVP with the implicit solvent model of water (SMD variation of IEFPCM).

## 4.6 | Cambridge Structural Database mining

Cambridge Structural Database version 5.44 (April 2023), with updates on June 23 and September 23, was queried using ConQuest 2023.2.0<sup>[33]</sup>; the results were analyzed visually in Mercury 2023.2.0<sup>[33]</sup> (both as parts of the CSD Portfolio software suites from The Cambridge Crystallographic Data Center). Then, the obtained values were statistically analyzed using pandas 1.4.3 in Python 3.10.5 and are reported as mean with minimum and maximum values.

### ACKNOWLEDGMENTS

Computational resources were supplied by the project “e-Infrastruktura CZ” (e-INFRA CZ LM2018140) supported by the Ministry of Education, Youth and Sports of the Czech Republic. Supported by the Ministry of Health of the Czech Republic, grant no. NU21-05-00482 (grant to J. Z.). V. S. K. P. acknowledges the funding support from the Grant Agency of Charles University with Project GA UK No. 349 721 and Charles University with Project SVV 260 666. The publication was supported by the research project 2200/04/2024-2026 as part of the “Competition for 2024-2026 Postdoctoral Job Positions at the University of Hradec Králové,” at the Faculty of Science, University of Hradec Králové (grant to M. J.). Open access publishing facilitated by Univerzita Karlova, as part of the Wiley-CzechELib agreement.

### CONFLICTS OF INTEREST STATEMENT

The authors declare no conflicts of interest.

### DATA AVAILABILITY STATEMENT

Data that supports the findings of this study are available in the Supporting Information of this article.

### ORCID

Vinod Sukanth Kumar Pallabothula  <http://orcid.org/0000-0002-3327-3078>

Matteo Mori  <https://orcid.org/0000-0002-7491-1494>

Ondřej Jandourek  <https://orcid.org/0000-0003-4633-2062>

Klára Konečná  <https://orcid.org/0000-0001-5670-7767>

Pavla Paterová  <https://orcid.org/0000-0003-0192-7345>

Martin Novák  <https://orcid.org/0000-0001-9692-7641>

Paulína Dudášová-Hatoková  <https://orcid.org/0000-0002-8075-101X>

Petra Štěrbová-Kovaříková  <https://orcid.org/0000-0002-1242-5706>

Carlo Castellano  <http://orcid.org/0000-0002-7497-0670>

Fiorella Meneghetti  <https://orcid.org/0000-0002-6511-7360>

Stefania Villa  <https://orcid.org/0000-0002-0636-7589>

Jiří Kuneš  <https://orcid.org/0000-0001-7257-0641>

Martin Juhás  <http://orcid.org/0000-0002-1890-9082>

Jan Zitko  <https://orcid.org/0000-0003-0104-9925>

### REFERENCES

- [1] B. Cheng, Z. Cai, Z. Luo, S. Luo, Z. Luo, Y. Cheng, Y. Yu, J. Guo, Y. Ju, Q. Gu, J. Xu, X. Jiang, G. Li, H. Zhou, *J. Med. Chem.* **2022**, *65*, 15840.
- [2] S. Jiang, Q. Zeng, M. Gettayacamin, A. Tungtaeng, S. Wannaying, A. Lim, P. Hansukjariya, C. O. Okunji, S. Zhu, D. Fang, *Antimicrob. Agents Chemother.* **2005**, *49*, 1169.
- [3] N. P. McLaughlin, P. Evans, M. Pines, *Bioorg. Med. Chem.* **2014**, *22*, 1993.
- [4] Y. Luo, X. Xie, D. Luo, Y. Wang, Y. Gao, *J. Leukoc. Biol.* **2017**, *102*, 1333.
- [5] A. Demiroglu-Zergeroglu, G. Turhal, H. Topal, H. Ceylan, F. Donbaloglu, K. Karadeniz Cerit, R. R. Odongo, *Cell Biol. Int.* **2020**, *44*, 1934.
- [6] I. Yoon, S. Kim, M. Cho, K. A. You, J. Son, C. Lee, J. H. Suh, D. J. Bae, J. M. Kim, S. Oh, *EMBO Mol. Med.* **2023**, *15*, e16940.
- [7] R. Adachi, K. Okada, R. Skene, K. Ogawa, M. Miwa, K. Tsuchinaga, S. Ohkubo, T. Henta, T. Kawamoto, *Biochem. Biophys. Res. Commun.* **2017**, *488*, 393.
- [8] K. Kurata, A. James-Bott, M. A. Tye, L. Yamamoto, M. K. Samur, Y.-T. Tai, J. Dunford, C. Johansson, F. Senbabaoglu, M. Philpott, C. Palmer, K. Ramasamy, S. Gooding, M. Smilova, G. Gaeta, M. Guo, J. C. Christianson, N. C. Payne, K. Singh, K. Karagoz, M. E. Stokes, M. Ortiz, P. Hagner, A. Thakurta, A. Cribbs, R. Mazitschek, T. Hideshima, K. C. Anderson, U. Oppermann, *Blood Cancer J.* **2023**, *13*, 12.
- [9] L. Pang, S. D. Weeks, M. Juhás, S. V. Strelkov, J. Zitko, A. Van Aerschot, *Int. J. Mol. Sci.* **2021**, *22*, 7793.
- [10] V. S. K. Pallabothula, M. Kerda, M. Juhás, O. Jandourek, K. Konečná, P. Bárta, P. Paterová, J. Zitko, *Biomolecules* **2022**, *12*, 1561.
- [11] A. K. Ghosh, M. Brindisi, *J. Med. Chem.* **2019**, *63*, 2751.
- [12] G. Bouz, M. Juhás, P. Niklová, O. Jandourek, P. Paterová, J. Janoušek, L. Tůmová, Z. Kovalíková, P. Kastner, M. Doležal, J. Zitko, *Molecules* **2017**, *22*, 1797.
- [13] L. Semelková, O. Jandourek, K. Konečná, P. Paterová, L. Navrátilová, F. Trejtnar, V. Kubiček, J. Kuneš, M. Doležal, J. Zitko, *Molecules* **2017**, *22*, 495.
- [14] H. Wamhoff, E. Kroth, *Synthesis* **1994**, *1994*, 405.

- [15] P. Jakobsen, A. M. Horneman, E. Persson, *Bioorg. Med. Chem.* **2000**, *8*, 2803.
- [16] P. Gopal, W. Nartey, P. Ragunathan, J. Sarathy, F. Kaya, M. Yee, C. Setzer, M. S. S. Manimekalai, V. Dartois, G. Grüber, T. Dick, *ACS Infect. Dis.* **2017**, *3*, 807.
- [17] H. L. Stewart, M. Bon, C. Wills, M. P. Martin, L. Z. Wang, E. S. Mackenzie, P. G. Waddell, M. J. Waring, *Bioorg. Med. Chem.* **2023**, *19*, 117387.
- [18] V. S. Bryantsev, T. K. Firman, B. P. Hay, *J. Phys. Chem. A* **2005**, *109*, 832.
- [19] G. Luchini, D. M. H. Ascough, J. V. Alegre-Requena, V. Gouverneur, R. S. Paton, *Tetrahedron* **2019**, *75*, 697.
- [20] A. V. Marenich, C. J. Cramer, D. G. Truhlar, *J. Phys. Chem. B* **2009**, *113*, 6378.
- [21] I. J. Bruno, J. C. Cole, M. Kessler, J. Luo, W. D. S. Motherwell, L. H. Purkis, B. R. Smith, R. Taylor, R. I. Cooper, S. E. Harris, A. G. Orpen, *J. Chem. Inf. Comput. Sci.* **2004**, *44*, 2133.
- [22] S. J. Cottrell, T. S. G. Olsson, R. Taylor, J. C. Cole, J. W. Liebeschuetz, *J. Chem. Inf. Model.* **2012**, *52*, 956.
- [23] M. A. Spackman, D. Jayatilaka, *CrystEngComm.* **2009**, *11*, 19.
- [24] O. Jandourek, M. Tauchman, P. Paterova, K. Konecna, L. Navratilova, V. Kubicek, O. Holas, J. Zitko, M. Dolezal, *Molecules* **2017**, *22*, 223.
- [25] J. Lin, Z. Zhang, X. Lin, Z. Chen, T. Luc, D. Zha, J. Wang, X. Xu, Z. Li, *Med. Chem.* **2022**, *18*, 353.
- [26] M. C. Burla, R. Caliendo, B. Carrozzini, G. L. Cascarano, C. Cuocci, C. Giacovazzo, M. Mallamo, A. Mazzone, G. Polidori, *J. Appl. Crystallogr.* **2015**, *48*, 306.
- [27] G. M. Sheldrick, *Acta Crystallogr., Sect. C: Struct. Chem.* **2015**, *71*, 3.
- [28] L. J. Farrugia, *J. Appl. Crystallogr.* **2012**, *45*, 849.
- [29] M. Nardelli, *J. Appl. Crystallogr.* **1995**, *28*, 659.
- [30] C. F. Macrae, I. Sovago, S. J. Cottrell, P. T. A. Galek, P. McCabe, E. Pidcock, M. Platings, G. P. Shields, J. S. Stevens, M. Towler, P. A. Wood, *J. Appl. Crystallogr.* **2020**, *53*, 226.
- [31] P. R. Spackman, M. J. Turner, J. J. McKinnon, S. K. Wolff, D. J. Grimwood, D. Jayatilaka, M. A. Spackman, *J. Appl. Crystallogr.* **2021**, *54*, 1006.
- [32] M. J. Frisch, G. W. Trucks, H. B. Schlegel, G. E. Scuseria, M. A. Robb, J. R. Cheeseman, G. Scalmani, V. Barone, G. A. Petersson, H. Nakatsuji, X. Li, M. Caricato, A. V. Marenich, J. Bloino, B. G. Janesko, R. Gomperts, B. Mennucci, H. P. Hratchian, J. V. Ortiz, A. F. Izmaylov, J. L. Sonnenberg, D. Williams-Young, F. Ding, F. Lipparini, F. Egidi, J. Goings, B. Peng, A. Petrone, T. Henderson, D. Ranasinghe, V. G. Zakrzewski, J. Gao, N. Rega, G. Zheng, W. Liang, M. Hada, M. Ehara, K. Toyota, R. Fukuda, J. Hasegawa, M. Ishida, T. Nakajima, Y. Honda, O. Kitao, H. Nakai, T. Vreven, K. Throssell, J. A. Montgomery Jr., J. E. Peralta, F. Ogliaro, M. J. Bearpark, J. J. Heyd, E. N. Brothers, K. N. Kudin, V. N. Staroverov, T. A. Keith, R. Kobayashi, J. Normand, K. Raghavachari, A. P. Rendell, J. C. Burant, S. S. Iyengar, J. Tomasi, M. Cossi, J. M. Millam, M. Klene, C. Adamo, R. Cammi, J. W. Ochterski, R. L. Martin, K. Morokuma, O. Farkas, J. B. Foresman, D. J. Fox, Gaussian, Inc., Wallingford, CT, **2016**.
- [33] I. J. Bruno, J. C. Cole, P. R. Edgington, M. Kessler, C. F. Macrae, P. McCabe, J. Pearson, R. Taylor, *Acta Crystallogr., Sect. B: Struct. Sci.* **2002**, *58*, 389.

### SUPPORTING INFORMATION

Additional supporting information can be found online in the Supporting Information section at the end of this article.

**How to cite this article:** V. S. K. Pallabothula, N. T. Abdalrahman, M. Mori, A. H. Fekri, O. Jandourek, K. Konečná, P. Paterová, M. Novák, P. Dudášová-Hatoková, P. Štěrbová-Kovářiková, C. Castellano, F. Meneghetti, S. Villa, J. Kuneš, M. Juhás, J. Zitko, *Arch. Pharm.* **2024**, e2400171.  
<https://doi.org/10.1002/ardp.202400171>